Experiments in Fluids 32 (2002) 458–471 © Springer-Verlag 2002
DOI 10.1007/s00348-001-0386-3

The effect of the expansion ratio on a turbulent non-Newtonian recirculating flow

A. S. Pereira, F. T. Pinho

Abstract Measurements of the mean and turbulent flow characteristics of shear-thinning moderately elastic 0.1% and 0.2% xanthan gum aqueous solutions were carried out in a sudden expansion having a diameter ratio of 2. The inlet flow was turbulent and fully developed, and the results were compared with data for water in the same geometry and with previous published Newtonian and non-Newtonian data in a smaller expansion of diameter ratio equal to 1.538. An increase in expansion ratio led to an increase in the recirculation length and in the axial normal Reynolds stress at identical normalised locations, but the difference between Newtonian and non-Newtonian characteristics was less intense than in the smaller expansion. An extensive comparison of mean and turbulent flow characteristics was carried out in order to understand the variation of flow features.

Nomenclature

C_T	static pressure variation coefficient
D	diameter of pipe downstream of sudden expansion (m)
d	diameter of pipe upstream of sudden expansion (m)
ER	expansion ratio
f_D	Darcy friction factor
h	step height (m)
K	consistency index in power law model (Pa^n)
k	turbulent kinetic energy (m^2/s^2)
L	recirculation bubble length (m)
n	power law index in power law and Sisko viscosity models
R	radius of pipe (m)
Re	Reynolds number
Re_w	Reynolds number based on wall viscosity in the upstream pipe
Re_{gen}	generalised Reynolds number
r	local radius (m)
r'	normalised radial coordinate, $r' = (r-R_1)/h$
U	axial bulk velocity (m/s)
u	local axial mean velocity (m/s)
u'_i	local root mean square of velocity component i (m/s)
U_o	axial centreline velocity (m/s)
U^+	local maximum velocity in the shear layer (m/s)
U^-	local minimum velocity in the shear layer (m/s)
u'	local root mean square of axial velocity (m/s)
v'	local root mean square of radial velocity (m/s)
w'	local root mean square of tangential velocity (m/s)
x	longitudinal coordinate (m)
β	shape factor for momentum
ε	parameter, $\varepsilon \equiv x_p/d$
$\dot{\gamma}$	shear rate (s^{-1})
η_{ref}	reference viscosity in the Sisko model (Pa)
η_∞	infinite shear rate viscosity in the Sisko model (Pa)
λ_S	time constant of Sisko viscosity model (s)
ρ	fluid density (kg/m^3)
σ	area ratio
μ	fluid viscosity (Pa)
μ_w	viscosity at the wall in the upstream pipe (Pa)

Subscripts

1	upstream (inlet) pipe
2	downstream pipe
ch	characteristic value
max	maximum values
p	pressure recovery

Received: 31 July 2000 / Accepted: 27 August 2001

A. S. Pereira
Departamento de Engenharia Química
Instituto Superior de Engenharia do Porto Rua de São Tomé
4200 Porto, Portugal

F. T. Pinho (✉)
Centro de Estudos de Fenómenos de Transporte,
DEMEGI, Faculdade de Engenharia,
Universidade do Porto, Rua Dr. Roberto Frias,
4200–465 Porto, Portugal
e-mail: fpinho@fe.up.pt

We would like to thank the financial support of the Stichting Fund of Schlumberger and project PBIC/C/CEG/2427/95 of Fundação para a Ciência e Tecnologia. The authors are also thankful to Instituto de Engenharia Mecânica e Gestão Industrial (INEGI) for providing lab facilities.

1 Introduction

Knowledge of non-Newtonian recirculating flows is still rather limited, although these are frequently encountered in the process industries. For dilute polymer solutions the flow is likely to be turbulent, but there are only a few quantitative studies available in the literature. Pak et al. (1991) measured the loss coefficient of polyacrylamide solutions in expansions having diameter ratios of 1.39 and 1.90 after a preliminary visualisation study (Pak et al. 1990) aimed at defining the ranges of laminar, transitional and turbulent regimes for various non-Newtonian fluids.

They concluded that the recirculation lengths of viscoelastic turbulent flows were longer than those involving purely viscous fluids, but the reasons were not fully understood. The lack of detailed information on the mean and turbulent flow fields in both works of Pak et al. motivated the more recent research.

The detailed velocity measurements of Castro and Pinho (1995) with tylose solutions, for turbulent fully developed inlet flow conditions, showed reductions of the normal Reynolds stresses of up to 30%, especially in the radial and tangential directions, but only small variations in the recirculation bubble. The more recent investigations of Pereira and Pinho (2000) with significantly more elastic fluids based on xanthan gum showed a shortening of the recirculation length and a mixed variation of the normal Reynolds stresses relative to the corresponding stresses for Newtonian fluids. To a large extent, the differences were attributed to the effect of viscoelasticity upon the Reynolds stress field in the upstream pipe, which was advected downstream. This was confirmed by the similar work of Escudier and Smith (1999), who probed the same solutions in the same geometry, but with a uniform low-turbulence inlet velocity profile. Although viscoelasticity reduced the turbulent kinetic energy, these changes were not sufficiently intense to strongly affect the mean flow.

It is necessary to pursue the detailed investigation of this class of flows in various ways: to extend it to other expansion ratios using the same fluids and to bring in significantly more elastic fluids, in particular those that were previously studied by Pak et al. (1991). This paper is a contribution to the first objective in that it extends the previous work of Pereira and Pinho (2000) to a larger sudden expansion with an expansion ratio (*ER*) equal to 2, using the same fluids.

Section 2 presents the experimental set-up and is followed by a brief description of the rheology of the fluids. Then, the hydrodynamic results are presented and discussed with the emphasis on the differences from previous measurements.

2 Experimental set-up

The flow configuration is the same as that used in the previous sudden expansion experiments by Pereira and Pinho (2000), except for the different transparent test section and downstream pipe. The rig consisted of a vertical closed loop with a 100-l tank and a centrifugal pump located at the bottom. The descending pipe before the test section was 26 mm in diameter and more than 90 diameters in length, leading to the sudden expansion from 26 mm to 52 mm in diameter and 630 mm in length. These dimensions thus define a diameter ratio of 1:2, in contrast to the ratio of 1:1.538 of Pereira and Pinho (2000). The 52-mm diameter pipe leads the flow back to the tank. The test section and coordinate system are represented schematically in Fig. 1. The test section had a square outer cross section to reduce diffraction of light beams and, to help ensure a fully developed flow at the inlet of the sudden expansion, a honeycomb was placed at the inlet of the descending 26-mm pipe, i.e., at more than 90 diameters upstream of the sudden expansion plane.

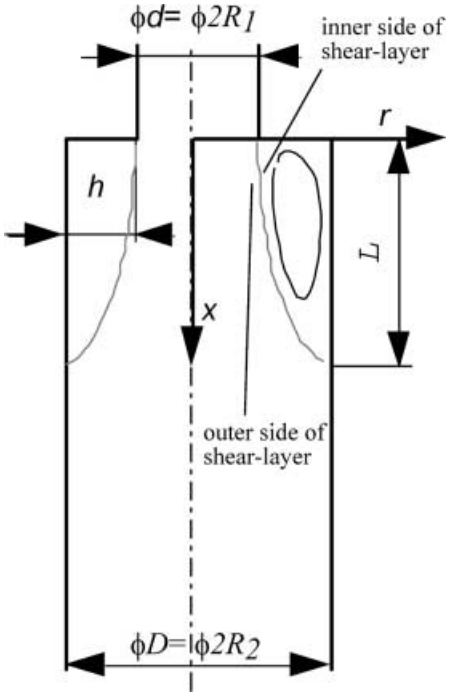

Fig. 1. Schematic representation of the sudden expansion test section and coordinate system

The rising pipe had an electromagnetic flowmeter (ABB Kent Taylor, Mag Master) and two valves that, together with a bypass circuit, allowed the flow rate to be properly monitored. The output signal from the flowmeter was transmitted to an 80386 PC via a data acquisition board (Keithley, Metrabyte DAS-8) interfaced with a multiplexer (Keithley, Metrabyte ISO 4). The measured flow rates were within 2% of the values computed from the velocity profiles when these were measured from wall to wall using laser-Doppler anemometry.

The anemometer was a miniaturised fibre-optic laser-Doppler velocimeter (INVENT, model DFLDA) similar to that described by Stieglmeier and Tropea (1992), with a 100-mm front lens mounted onto the 30-mm diameter probe. Scattered light was collected by a photodiode in the forward scatter mode. The main characteristics of the anemometer are listed in Table 1. Measurements of the radial velocity component were limited to the inner 70% of the pipe radius due to excessive refraction of light beams outside that region.

The signal was processed by a counter (TSI 1990C) interfaced with a computer via a DOSTEK 1400 A card, which provided the statistical quantities. The data

Table 1. Laser-Doppler characteristics

Laser wavelength	827 nm
Laser power	100 mW
Measured half-angle of beams in air	3.68°
Size of measuring volume in water (e^{-2} int.)	
Minor axis	37 μm
Major axis	550 μm
Fringe spacing	6.44 μm
Frequency shift	3.0 MHz

presented in this paper have been corrected for the effects of the mean gradient broadening. The maximum uncertainties in the axial mean and root mean square (rms) velocities at a 95% confidence level are 1.0% and 2.2% on axis, respectively, and 1.1% and 5.2% in the wall region, respectively. The uncertainties of the radial and tangential rms velocity components are 2.5% and 5.9% on axis and close to the wall, respectively.

In Sect. 4, the turbulence results are presented as normalised Reynolds stresses $u_i'^2/U_1^2$, and the corresponding uncertainties $\left(\Delta\left(u_i'^2/U_1^2\right)\right)$ are calculated with the root mean square rule (1), using the above values as input. The uncertainties range from 5% on axis to 11% at the wall.

$$\frac{\Delta\left(\frac{u_i'^2}{U_1^2}\right)}{\frac{u_i'^2}{U_1^2}} = \sqrt{4\left(\frac{\Delta u_i'}{u_i'}\right)^2 + 4\left(\frac{\Delta U_1}{U_1}\right)^2} \quad . \tag{1}$$

The velocimeter was mounted on a milling table with movement in the three coordinates and positional uncertainties of ±200 μm and ±150 μm in the axial and transverse directions, respectively.

Twenty-eight pressure taps were located on the pipe downstream of the sudden expansion and two taps were drilled upstream, in the region of fully developed flow, as described in more detail in Pereira (2000). The pressure variation in the sudden expansion was measured by means of differential pressure transducers (Validyne, models P305D S20 and S24); their outputs were sent to a computer via one of the four channels of the same data acquisition board used for the flow rate measurements. The overall uncertainty of the pressure measurements varied between 1.6% and 7.2% for high and low pressure differences, respectively.

Heating and cooling circuits in the reservoir were used to control and maintain the temperature at a constant 25 °C ± 0.5 °C.

3
Fluid properties

Water and aqueous solutions of xanthan gum (Kelco, grade Keltrol TF), a polysaccharide of high molecular weight (2×10^6 kg/kmol), at weight concentrations of 0.1% and 0.2% were used. These were the same fluids used previously by Pereira and Pinho (1999, 2000), who reported on their rheology. Tap water was used to prepare the solutions, with the addition of 0.02 wt.% of a biocide (Rohm and Haas, Kathon LXE) to help prevent bacteriological degradation. The solutions were shear thinning over a wide range of shear rates. The rheological characterization was carried out in a rheometer (Physica MC100) implementing a double-gap concentric cylinder geometry, described by Coelho and Pinho (1998).

The viscometric viscosity of the solutions is plotted in Fig. 2 together with the curve-fitting Sisko model equation (2), whose parameters are listed in Table 2.

$$\eta = \eta_{\mathrm{ref}}(\lambda_s\dot{\gamma})^{n-1} + \eta_\infty \quad . \tag{2}$$

Creep and oscillatory shear flows were used to characterize the extent of viscoelastic behaviour. A similar

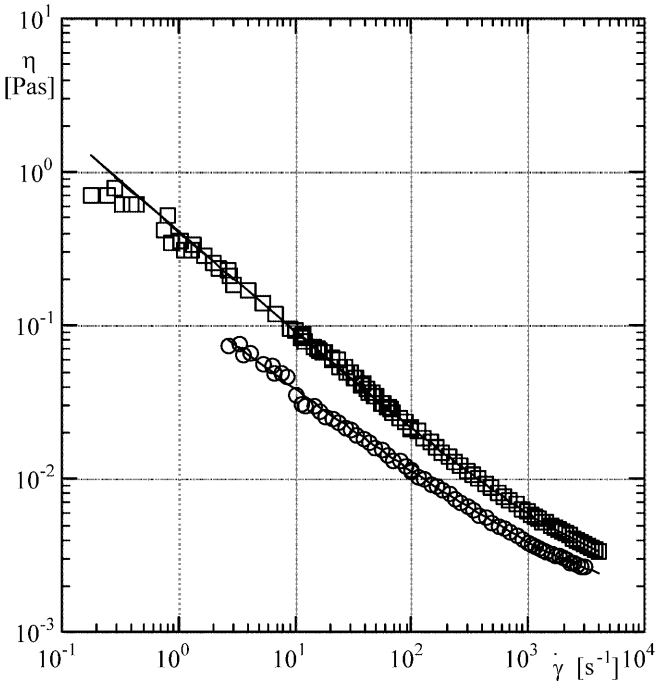

Fig. 2. Variation of the viscosity of xanthan gum solutions with the shear rate at 25 °C, and the corresponding curve-fit Sisko models: ○ 0.1% xanthan gum; □ 0.2% xanthan gum. From Pereira and Pinho (2000)

Table 2. Sisko model parameters for Keltrol solutions at 25 °C. From Pereira and Pinho (2000)

Solution	η_{ref} (Pa)	η_∞ (Pa)	λ_s (s)	n
0.1%	10.52	0.0012	1970	0.4299
0.2%	58.06	0.001589	1900	0.3434

aqueous solution of 0.2% XG (same grade) was also investigated in a sudden expansion by Escudier and Smith (1999), where other rheological measurements, such as the first normal stress difference, are reported. The only difference between the 0.2% XG solutions used here and those used by Escudier and Smith was the solvent, which was local tap water in both cases. The differences in rheology were fairly small and are extensively assessed in the comparative works of Escudier et al. (1998, 2001).

Prior to the investigation of the sudden expansion flow, the fully developed turbulent pipe flow was studied in terms of friction factor versus Reynolds number behaviour by Pereira and Pinho (1999). The solutions exhibited drag reduction in the 26-mm diameter upstream pipe. For maximum wall Reynolds numbers of 40,100 and 28,100, the measured drag reductions of 45% and 59% for the 0.1% and 0.2% xanthan gum solutions represent over 50% and 75%, respectively, of the maximum drag reduction predicted by Virk's asymptote (Virk et al. 1970).

4
Results and discussion

Measurements of the three components of the mean and root mean square of the fluctuations of the velocity of the

xanthan gum solutions and water were carried out by means of laser-Doppler velocimetry in the ER=2 sudden expansion. Table 3 compares these measurements with those of the previous work of Pereira and Pinho (2000) for the ER=1.538 expansion using the same fluids. The flow conditions were the same as in Pereira and Pinho (2000), i.e., similar fully developed inlet conditions and equal Reynolds numbers when based exclusively on the upstream pipe flow (Re_w and Re_{gen}). Table 3 lists the flow conditions, the normalised recirculation length (L/h) and the maximum values of the normal Reynolds stresses and turbulence kinetic energy k.

Three Reynolds numbers are used to characterize the flow conditions: the upstream pipe Reynolds number Re_w based on the wall viscosity, the upstream pipe generalised Reynolds number Re_{gen}, and the Reynolds number Re presented by Castro and Pinho (1995). In this work, the step height h and the inlet pipe bulk velocity U_1 are used to define a characteristic shear rate U_1/h at which the viscosity is determined. While Re_w and Re_{gen} have the same values in both geometries because they refer to the same upstream flow and are independent of downstream conditions, the value of Re is smaller for ER=2 than for ER=1.538 due to the impact of the larger step height on the characteristic shear rate.

4.1 Inlet flow

The inlet flow was measured at $0.65d$ upstream of the expansion plane. Here, as reported in detail by Pereira (2000) for Newtonian fluids, both mean axial velocity profiles agree with the logarithmic law ($u^+=2.5\ln y^+ + 5.5$). The turbulent profiles, which are normalised by the friction velocity, compare favourably with the results of Lawn (1971).

The Newtonian and non-Newtonian turbulent flow inlet conditions are compared in the plots of Fig. 3. The non-Newtonian results are typical of fluids exhibiting drag reduction (Pinho and Whitelaw 1990): the axial Reynolds normal stress is slightly lower than that of Newtonian flows over 80% of the radius, but exceeds the Newtonian stresses at the wall region, whereas the radial and tangential normal stresses are greatly attenuated. The dampening of the transverse turbulence, as well as the drag reduction intensity in pipe flow, increase with polymer concentration (Pereira and Pinho 1999).

It is important to emphasize that, in the wall region, the solutions of xanthan gum have higher axial normal Reynolds stresses than the water flows, which has an impact on the flow downstream of the expansion plane.

4.2 Expansion mean flow

Downstream of the expansion, the Newtonian results are consistent with the findings of Khezzar et al. (1985) and Pak et al. (1990), as shown in the comparison between recirculation lengths of Fig. 4. At high Reynolds numbers the normalised recirculation length increases weakly with the expansion ratio and decreases, also weakly, with Reynolds number.

The results of the recirculation length measurements for the polymer solutions are plotted in Fig. 5. As in the smaller expansion, the addition of polymer reduced the recirculation length relative to that of the pure Newtonian solvent. For the ER=2 expansion, the reduction in L/h with the change from water to 0.1% XG is 10%, which is half that found by Pereira and Pinho (2000) for the smaller expansion. A further increase in xanthan gum concentration to 0.2% has a small effect on the reduction of the recirculation length. Note that for the smaller expansion, the L/h value of the 0.1% XG solution is intermediate to those of the two runs with 0.2% XG. This is in contrast to the case for the ER=2 geometry, which is attributed to the measurement uncertainty. The data of Escudier and Smith (1999) for the same fluid in the smaller expansion corresponds to a uniform velocity inlet with low turbulence. Their recirculation region is longer than for fully developed inlet flow in the same geometry because its lower turbulence, downstream of the expansion, reduces the spreading rate of the shear layer, as explained by Pereira and Pinho (2000).

The smaller polymer effect on L/h for the case of ER=2 is in agreement with a higher rate of variation of the vorticity thickness (δ_ω), which is defined as

$$\delta_\omega = \frac{U^+ - U^-}{\left(\frac{\partial u}{\partial r}\right)_{\max}} \quad , \tag{3}$$

where U^+ and U^- represent the local maximum and minimum velocities in the shear layer, here assumed to be the centreline velocity U_0 and zero, respectively.

Table 3. Flow conditions, recirculation length and maximum turbulent quantities

Run	Fluid	U_1 (m/s)	Re	Re_w	Re_{gen}	L/h	$\left(\overline{u'^2}/U_1^2\right)_m$	$\left(\overline{v'^2}/U_1^2\right)_m$	$\left(\overline{w'^2}/U_1^2\right)_m$	$\left(k/U_1^2\right)_m$
1*	Water	4.61	135,000	135,000	135,000	8.43	0.047	0.028	0.033	0.053
2*	Water	1.73	50,300	50,300	50,300	8.71	0.042	0.027	0.028	0.048
3*	0.1% XG	3.04	14,200	19,600	8,100	6.93	0.040	0.025	0.032	0.048
4*	0.2% XG	5.10	19,000	27,200	10,700	6.78	0.050	0.026	0.033	0.054
5*	0.2% XG	4.05	13,400	19,400	7,700	7.14	0.045	0.024	0.033	0.050
1**	Water	4.62	134,000	134,000	134,000	9.30	0.056	0.026	0.034	0.056
2**	Water	1.74	50,400	50,400	50,400	10.00	0.053	0.024	0.028	0.052
3**	0.1% XG	3.05	10,500	19,600	8,100	9.08	0.048	0.025	0.030	0.049
4**	0.2% XG	5.05	13,000	27,100	10,600	8.73	0.051	0.025	0.031	0.051
5**	0.2% XG	4.04	9,200	19,400	7,700	8.77	0.049	0.025	0.031	0.051

* D/d=1.538 from Pereira and Pinho (2000)
** New data for D/d=2.0

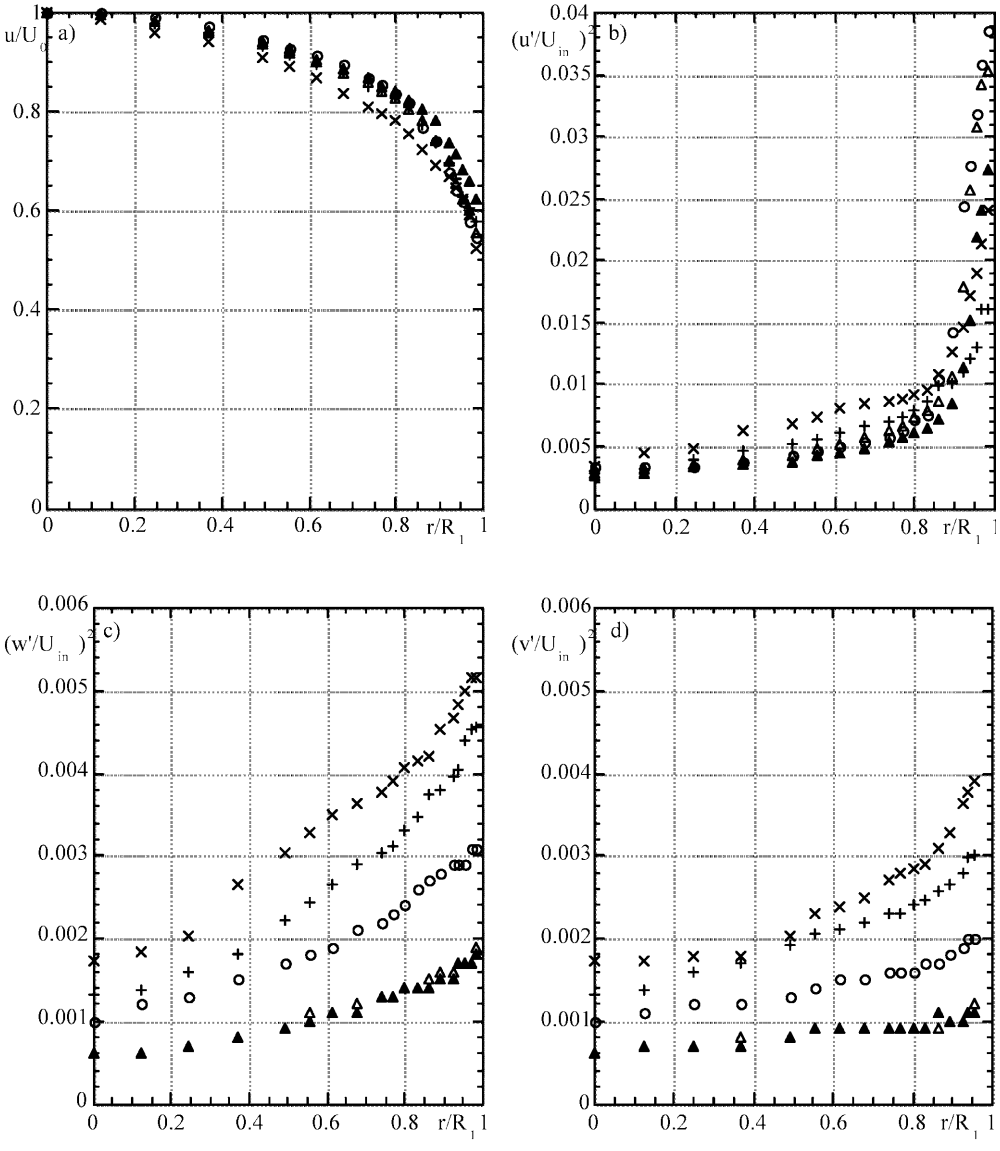

Fig. 3a–d. Radial profiles of the inlet mean and turbulent flow conditions at x/d=–0.65: **a** u/U_0; **b** $(u'/U_{in})^2$; **c** $(w'/U_{in})^2$; **d** $(v'/U_{in})^2$. × Water, Re=54,000; + Water, Re=134,000; ○ 0.1% XG, Re=19,600; △ 0.2% XG, Re=19,400; ▲ 0.2% XG, Re=27,100

For the ER=1.538 expansion Pereira and Pinho (2000) found that δ_ω varied linearly with the longitudinal coordinate according to

$$\frac{\delta_\omega}{d} = 0.15\frac{x}{d} + 0.1 \quad , \tag{4}$$

where d represents the inlet pipe diameter. For the larger (ER=2) expansion, the variation of δ_ω/d is no longer linear, as can be seen in Fig. 6. Although the growth of the vorticity thickness is initially fast, it becomes linear with a slope of 0.16 in the range $0.75 \le x/d \le 2$ and later decreases because of the effects of shear layer curvature and wall proximity. A more appropriate law of variation of the vorticity thickness is of second order

$$\frac{\delta_\omega}{d} = 0.09 + 0.24\frac{x}{d} - 0.025\left(\frac{x}{d}\right)^2, \tag{5}$$

and is also plotted in Fig. 6. This change in the behaviour of the vorticity thickness is a consequence of the lower degree of confinement and higher curvature of the shear layer for the ER=2 geometry relative to the smaller expansion.

Figure 7a compares the downstream mean flow field of the 0.1% xanthan gum solution with that of the water flows, whereas Fig. 7b compares the Re=50,000 water flow with the two 0.2% xanthan gum flows. The lines in the figures represent the location of zero axial mean velocity. The mean flows are all similar, with differences only detected in detailed comparisons. Early within the recirculation region, the velocities of the xanthan gum solutions are more negative than those of the water flows, but that is reversed for x/d>2.5, in agreement with the shorter lengths shown by the non-Newtonian flows. Also, in the early stages of the downstream flow, the xanthan gum mean axial velocity profiles are flatter in the central core than those of the water: note their lower velocities for r/R<0.3 and higher velocities for $0.3 \le r/R \le 0.5$. The more negative velocities in the recirculation region and the flatter profiles in the central core result in higher mean velocity gradients in the shear layer for the polymer flows, which contributes to higher production of the u'^2 Reynolds stress there, as observed previously for the ER=1.538 case.

Further downstream, the differences in the mean velocity profile in the central region remain, as the flow

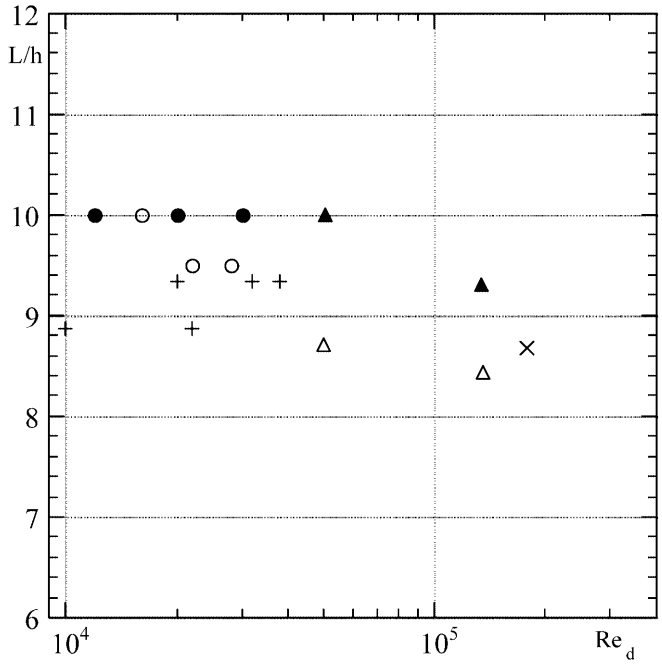

Fig. 4. Effect of expansion ratio and Reynolds number on normalised recirculation length for Newtonian fluids: + D/d= 1.75, Khezzar et al. (1985); ● D/d=2.0, O D/d= 2.667, Pak et al. (1990); × D/d=1.538, Castro and Pinho (1995); △ D/d=1.538, Pereira and Pinho (2000); ▲ D/d=2.0, present work

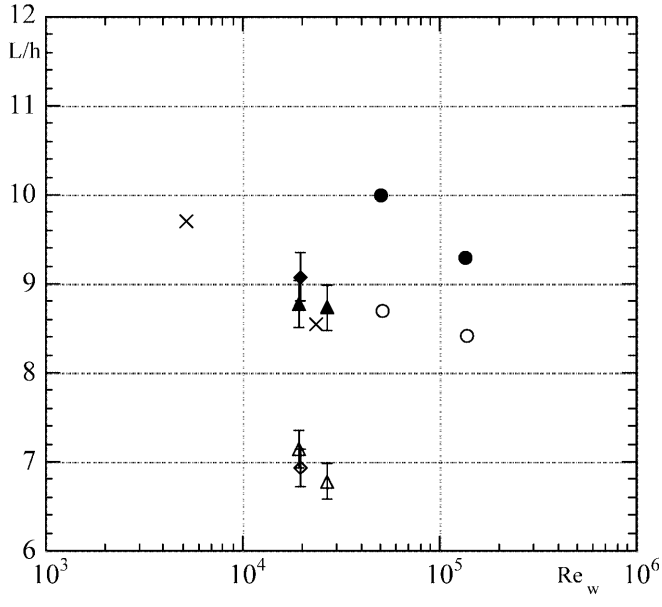

Fig. 5. Effect of expansion ratio and upstream wall Reynolds number on normalised recirculation length with 3% error bars: ○ water; ◊ 0.1% XG; △ 0.2% XG. *Open symbols*: *ER*=1.538; *Closed symbols*: *ER*=2; × 0.2% XG in *ER*=1.538 from Escudier and Smith (1999)

tends to a fully developed condition. In the fully developed condition, the normalised velocity on axis is lower than for the water flow, as already happened in the upstream pipe (Pereira and Pinho 2000).

The measurements of the wall static pressure allowed the determination of the static pressure variation coefficient

$$C_T \equiv \frac{p - p_0}{\frac{1}{2}\rho U_{in}^2}, \tag{6}$$

where p_0 is the reference pressure measured in the last tap of the upstream pipe, just upstream of the sudden expansion plane. The variation of C_T with x/h and x/L is plotted in Fig. 8a, b. Figure 8a shows that pressure recovery requires a longer length (x_p=εd with $\varepsilon \sim$ 11–12), in contrast to the smaller expansion where $\varepsilon \sim$ 8–10 (depending on the fluid) as reported by Pereira and Pinho (2000). However, this is misleading, and proper normalisation of x_p shows that, in fact, pressure recovery is faster in the larger expansion.

A better collapse of the pressure coefficient data is obtained in Fig. 8b, where the recirculation length is now used as the normalising geometrical factor. The maximum gradient of pressure coefficient takes place at $x/L \approx 1$, where the main body of fluid experiences the most intense radial flow deceleration created by the expansion. The pressure data also confirms, indirectly and independently, the trends observed for the recirculation length as a function of fluid type and Reynolds number. The arrangement of L in Table 3 is the same as the arrangement of the C_T curves in the high-gradient region in Fig. 8a, so that normalisation with L leads to collapse of data in this region.

Pressure recovery location x_p can be normalised as $x_p/h = \varepsilon d/h$, giving values of $x_p/h \sim$ 22 to 24 for *ER*=2 and $x_p/h \sim$ 29.7 to 37.1 for *ER*=1.538. As suggested by Fig. 8b, it is probably more adequate to normalise x_p with the recirculation length, i.e., $x_p/L = \varepsilon \frac{h}{L}\frac{d}{h}$. Recovery of C_T now takes place at about $x_p/L \sim$ 2.5 for all flows in the larger expansion, which is less than the value of 4.2 seen in the smaller

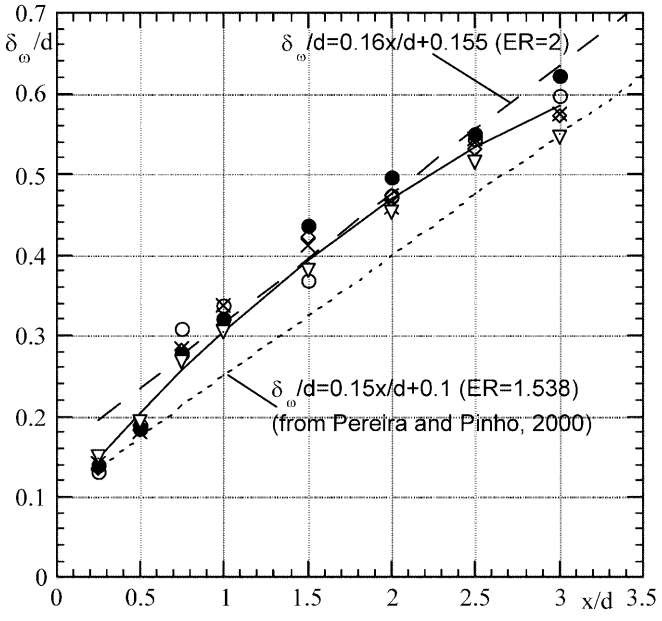

Fig. 6. Longitudinal variation of the vorticity thickness: × water, *Re*=50,400; ▽ water, *Re*=134,000; ◊ 0.1% XG, *Re*=19,600; ○ 0.2% XG, *Re*=27,100; ● 0.2% XG, *Re*=19,400. *Solid line* from (4)

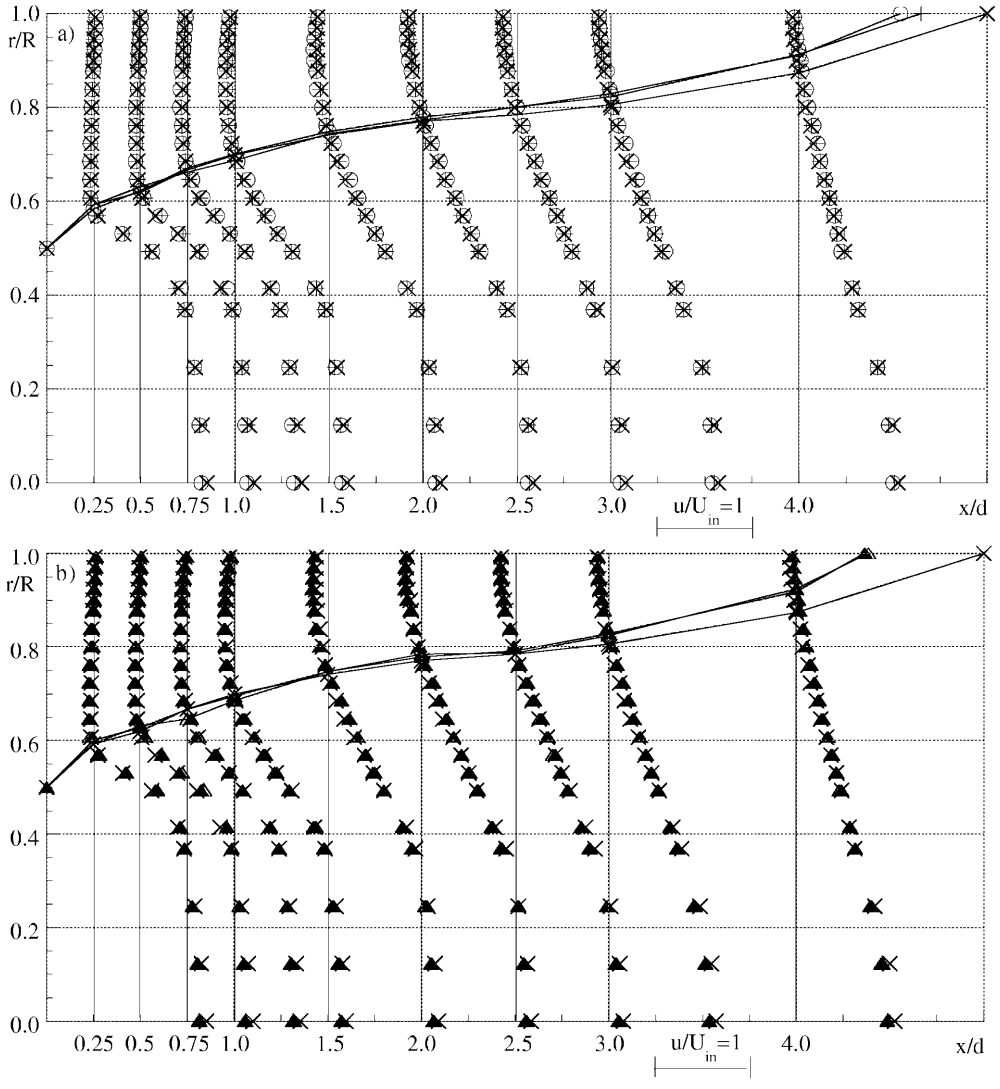

Fig. 7. **a** Normalised mean velocity profiles: × water, Re=50,400; + water, Re=134,000; ○ 0.1% xanthan gum, Re_w=19,600; **b** Normalised mean velocity profiles: × water, Re=50,400; △ 0.2% xanthan gum, Re_w=19,400; ▲ 0.2% xanthan gum, Re_w=27,100

expansion. Using both normalisations, recovery is indeed quicker in the larger expansion. The apparent controversy stems from the fact that there is only a small effect of the expansion ratio on L/h and x_p/d (both increased about 20% when ER increased by 30%), but a large effect upon the ratio d/h required to convert x_p/d into x_p/h or x_p/L.

To help quantify the maximum amount of recovery, Fig. 8b includes the theoretical static pressure coefficient C_T given by

$$C_T = 2\beta_1\sigma\left(1 - \frac{\beta_2}{\beta_1}\sigma\right), \qquad (7)$$

where $\sigma=(d/D)^2$ and β_1 and $\underline{\beta_2}$ are fully developed momentum shape factors ($\beta \equiv \overline{u^2}/\bar{u}^2$ with the overbar denoting an area average) upstream and downstream of the expansion. The upstream momentum shape factors were calculated from the mean velocity profiles measured at $x/d\approx$–0.65 and are listed in Table 4.

As seen in Fig. 3a, the inlet axial mean velocity profile is more uniform for the high Reynolds number water flow and the flatness of the profile is reduced when the Reynolds number decreases and/or the polymer concentration increases.

The static pressure variation coefficient is rather sensitive to β_1. The theoretical value of C_T for uniform inlet and outlet profiles (β=1) is 0.375, which is increased by an average 4% when the true value of β_2 is considered, assuming the downstream fully developed profile has the same shape as the upstream profile ($\beta_2 = \beta_1$). This is probably not the case except for the water flows, because these xanthan gum solutions are drag reducing (Pereira and Pinho 1999) by an amount less than the maximum predicted by Virk. It is well known that in such cases the flow hydrodynamics still depend on pipe diameter (Virk 1975). However, this is not important here because C_T is not very sensitive to the ratio β_2/β_1.

The two horizontal lines in Fig. 8b represent the theoretical C_T for a uniform inlet and outlet (C_T=0.375) and C_T=0.390, where the latter value is an average of C_T values from Table 4 that considers the true inlet shape factor. The measured value of C_T exceeds the theoretical values of C_T in all cases because of the role of the wall shear stresses. In the range $0<x/L\leq1$ the flow is reversed, the stress is positive and so it contributes to a pressure rise. For $1<x/L\leq2$ the flow at the wall is in the direct sense, the stress is negative and it contributes to a decrease in the pressure.

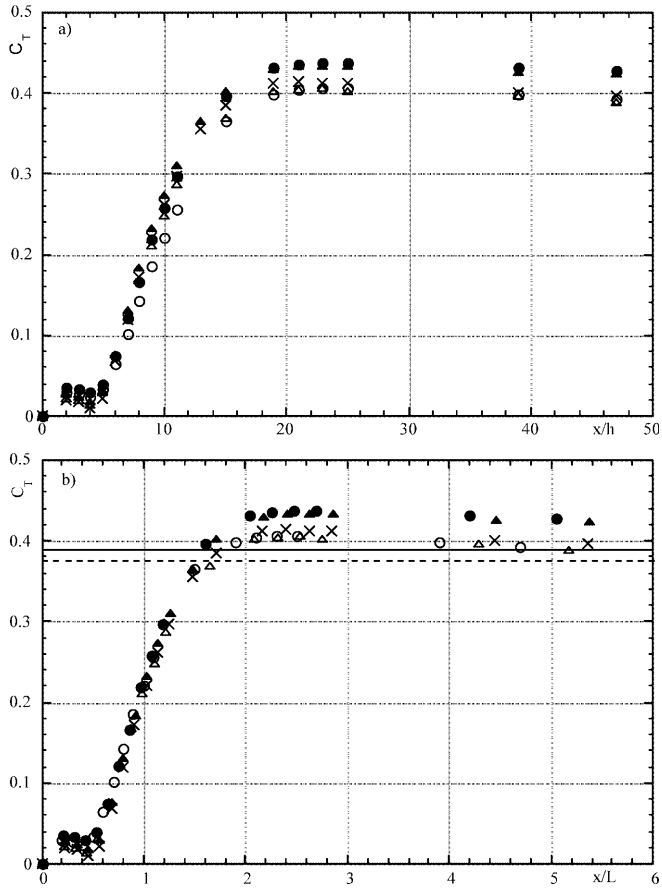

Fig. 8. Variation of static pressure coefficient as a function of x/h (a) and x/L (b): ○ water at Re_w=50,040; ● water at Re_w=134,000; △ 0.1% XG at Re_w=19,600; ▲ 0.2% XG at Re_w=27,100; × 0.2% XG at Re_w=19,400; *solid line* from (6) with $\beta_1=\beta_2=1$; *dashed line* from (6) with $\beta_1=\beta_2=1.039$ (average value from Table 4)

However, C_T is still increasing significantly, an indication that the axial mean velocity is under strong deceleration, and spreading radially, which suggests that the wall shear rates, and consequently, the shear stresses, are rather low and insufficient to compensate for the increased pressure due to positive stress in the recirculation region. This argument is somewhat reinforced by the very slow decay of C_T downstream of x/L=3, which is now basically due to the effect of wall friction. Thus, the overall effect of wall stress up to x/L of 2.5 is an increased pressure contribution from the reversed flow and hence the measured values of C_T are higher than the theoretical values.

4.3
Expansion turbulent flow

In terms of the turbulent flow field, the findings for the ER=2 geometry are qualitatively the same as those of Pereira and Pinho (2000) for the ER=1.538 expansion. In the upstream fully developed pipe flow, the addition of polymer resulted in higher axial normal Reynolds stresses in the wall region, but lower radial and tangential stresses all across the pipe. The immediate consequence of this inlet condition is that advection by the mean flow of this high near-wall axial turbulence to the shear layer downstream of the expansion plane (here referred to as the near shear layer) together with the higher $\overline{u'^2}$ production at the initial stages of the downstream flow, resulted in the earlier occurrence of the region of peak axial turbulence in the near shear layer than for Newtonian flows. This earlier development of high turbulence downstream of the expansion was responsible for the shorter recirculation region of the non-Newtonian flows.

Table 4. Momentum shape factor β_1 in the fully developed upstream profile measured at x/d=–0.65 and corresponding C_T assuming $\beta_1=\beta_2$

Fluid	Re_w	β_1	C_T
Water	134,000	1.033	0.387
Water	50,400	1.039	0.390
0.1% XG	19,600	1.036	0.389
0.2% XG	27,100	1.037	0.389
0.2% XG	19,400	1.044	0.392

A first conclusion on the expansion effect can be drawn from the data in Table 3: the maximum axial turbulence increases by about 20% for an increase of 30% in expansion ratio, which is mirrored by increases of 20% in x_p/d and L/h discussed in Sect. 4.2. This is consistent with the findings of Khezzar et al. (1985), who reported increases of 30% in axial turbulence for an increase of 35% in expansion ratio for Newtonian fluids. Similarly, Pronchick and Kline (1983) found the same for plane expansions. With the exception of the 0.2% XG flow at Re_w=27,100, the axial turbulence of the non-Newtonian fluids also increased with the expansion ratio. For the radial and tangential turbulence the effect of expansion ratio is less intense, both for the Newtonian and non-Newtonian fluids.

The different scales of the two expansions require that comparisons be made carefully. First, in Fig. 9 we present some representative profiles of the measured axial and tangential normal Reynolds stresses using normalised absolute coordinates. That is, the radial position r is normalised by the downstream pipe radius R_2 and the data from the two expansions are compared at identical values of x/d. Plots of $\overline{v'^2}$ are not included for reasons of space, but they convey similar qualitative information as the plots of $\overline{w'^2}$.

This figure shows that the turbulence in the smaller expansion is higher than in the ER=2 case for all the normal components of the Reynolds stress tensor except $\overline{u'^2}$ at x/d. For instance, in Fig. 9a the progression of the difference between the maximum values of $\bar{u}'^2/U_1^2$ in the smaller and larger expansions is 5%, 30% and 23% at 0.5d, 1.0d and 1.5d, respectively. For the transverse component $\bar{w}'^2/U_1^2$ the effect is larger, and differences of 30%, 40% and 30% were measured in the same locations, respectively. These differences are maintained for the 0.1% XG flow of Fig. 9-b), but increase further for 0.2% XG at Re=27,000, where they can be as large as 50% for $\bar{u}'^2/U_1^2$.

However, these differences are misleading in that a given measuring station, say $x/d = 1.0$, corresponds to different axial locations in terms of the relevant dimension, the step height. In Sect. 4.2 it was shown that the

recirculation length is more adequately normalised by the step height and, as an example, in high Reynolds number Newtonian flows L/h tends to a constant value. It thus seems appropriate to compare flow fields at identical values of x/h, instead, except at the near shear layer, just downstream of the expansion plane, where the flow is not yet affected by the recirculating flow. Here the specific comparison of Fig. 9a with Fig. 9b at x/d=0.25 shows the earlier development of $\bar{u}'^2$ for xanthan gum in comparison with the water flows.

The comparisons in Fig. 9 are also made more difficult by the different radial positions of the shear layer; the upstream pipe wall is located at R_1/R_2=0.65 and 0.5 for the small and large expansions, respectively. The region downstream of the expansion plane can be made to coincide geometrically in nondimensional terms by normalising the radius as $r' \equiv (r - R_1)/h$ so that, regardless of the expansion ratio, the value of r' corresponding to locations downstream of the wall varies from 0 to 1.

Using these other geometrical normalisations for the axial and radial coordinates, some representative transverse profiles of the axial and tangential Reynolds stresses, akin to those of Fig. 9, were drawn in Fig. 10. Note that for the other two flows the corresponding figures show similar trends.

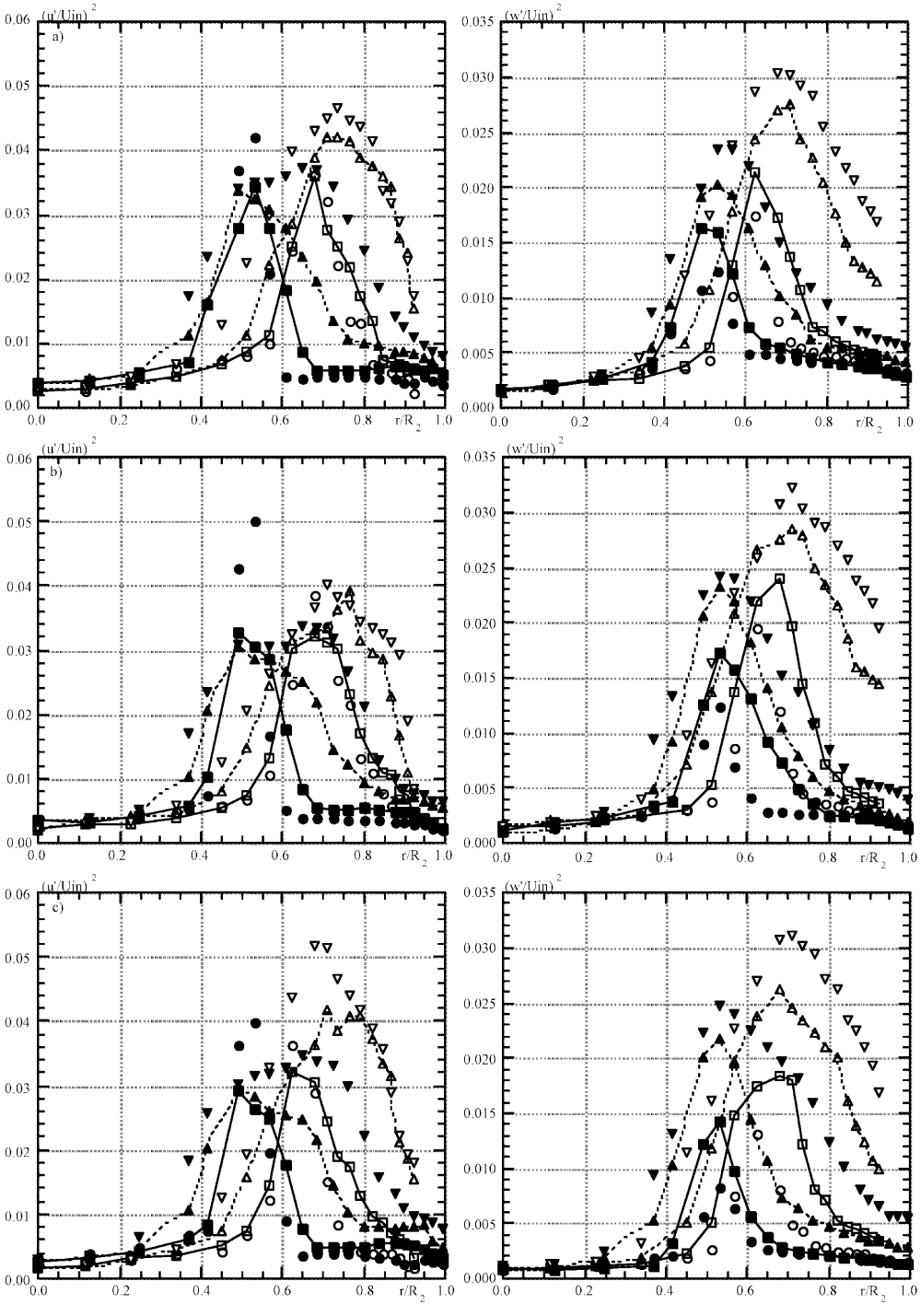

Fig. 9a–c. Radial profiles of the axial and tangential normal Reynolds stress as a function of downstream location x/d: **a** Water, Re=134,000; **b** 0.1% XG, Re=19,600; **c** 0.2% XG, Re=27,000 for x/d: ○ 0.25; □ 0.5; △ 1.0; ▽ 1.50. *Open symbol*: ER=1.538, *Closed symbol*: ER=2

The actual measurements in both geometries were carried out at the same values of x/d, so in order to plot Fig. 10 the data for ER=2 was linearly interpolated to obtain profiles at identical values of L/h as in the ER=1.538 expansion. Careful inspection of this figure now shows several features.

First, for all fluids the axial turbulence now reaches higher values in the ER=2 expansion than in the ER=1.538 case. The maximum $\overline{u'^2}$ occurs at around x/h≈5.57 downstream of the expansion plane, at r'≈0.4 and 0.2 from the corner for the larger and smaller expansions, respectively. The higher values of turbulence, especially in the near shear layer, mean that turbulence develops earlier in the ER=2 expansion.

The maximum normalised $\overline{u'^2}$ for the water flows in the larger expansion, at x/h≈5.57, are around 10% higher than the corresponding xanthan gum values. However, at lower values of x/h the levels of axial turbulence are similar for all fluids except at $x/h = 0.93$, where the radial profile of $\overline{u'^2}/U_1^2$ in the smaller expansion shows values higher by 50% to 100% than in the larger expansion. This difference occurs on the recirculation side of the shear-layer.

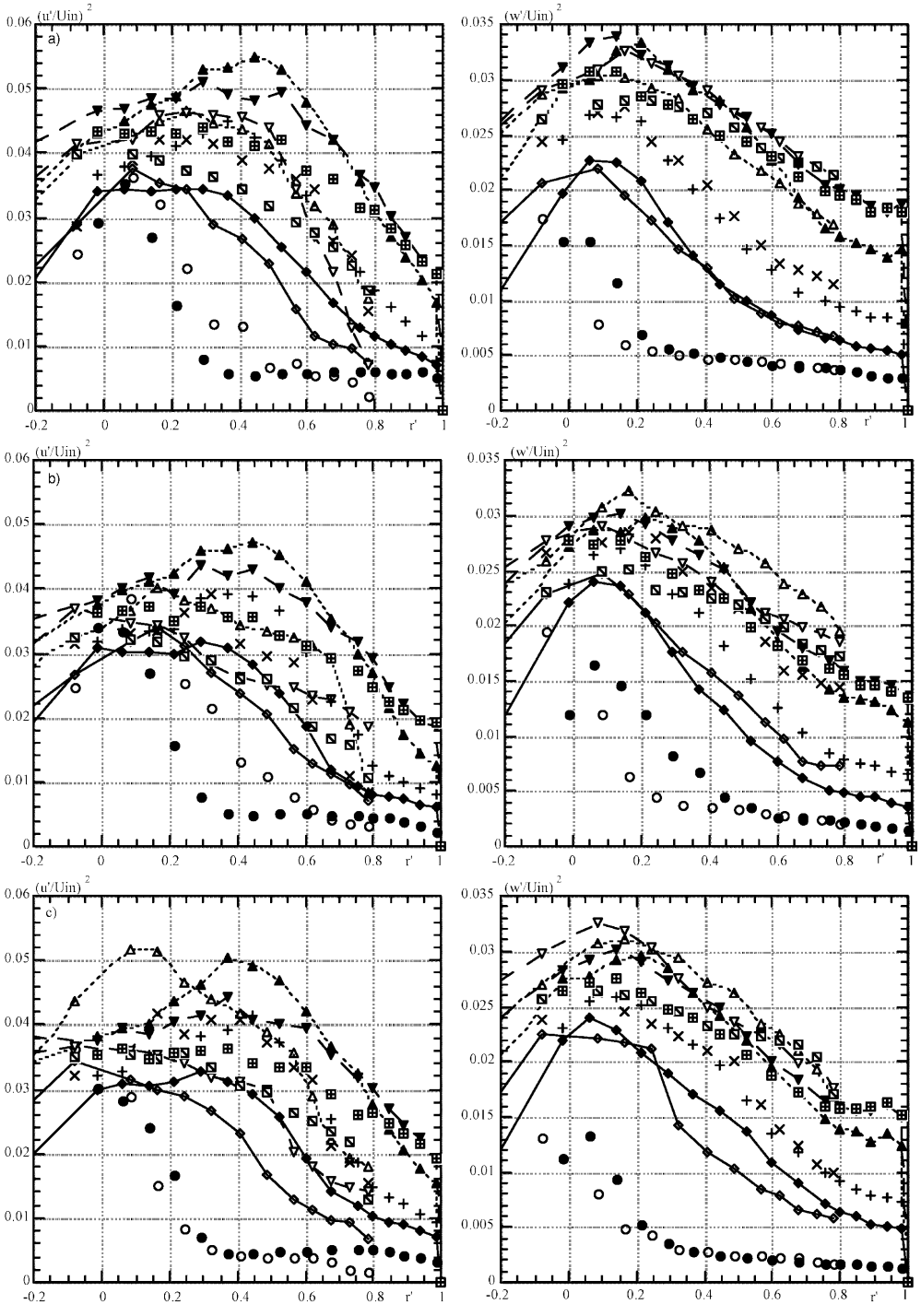

Fig. 10a–c. Radial profiles of the axial and tangential normal Reynolds stress as a function of downstream location x/h: **a** Water, Re=134,000; **b** 0.1% XG, Re=19,600; **c** 0.2% XG, Re=27,000 for x/h: ○ 0.93; ◇ 2.79; ×, + 3.71; △ 5.57; ▽ 7.43; ▣ and ⊞ 9.3. *Open/first symbol*: ER=1.538, *Closed/second symbol*: ER=2

On moving downstream the axial turbulence tends to peak at progressively higher values of r', following the spread and curvature of the shear layer towards the reversed flow region, but for $\overline{w'^2}$ the peak turbulence occurs always close to r'=0. The peak axial Reynolds stress follows the outer edge of the shear layer, whereas the peak tangential stress occurs roughly along the midline of the shear layer. This can be better seen with the help of the contours of the three normal Reynolds stresses for the *ER*=2 expansion in Figs. 11–13. For Newtonian fluids, the behaviour of the tangential turbulence in the relative coordinate normalisation of Fig. 10 is very similar in both expansions, whereas for the xanthan gum (Fig. 10b and c) there is a mixed behaviour. Although the maximum values of $\overline{w'^2}/U_1^2$ are very similar in both geometries, in the outer edge of the shear layer we observe a difference, with higher values alternating from the smaller to the larger expansion (c.f. the profiles for xanthan at x/h=2.79). Notice that the data plotted in Fig. 10 pertains to the region limited by the expansion plane and the end of the recirculation.

Within $x/h = 3.7$ of the expansion plane there is another difference in the locations of the peak values of the normal Reynolds stresses of the two geometries. For Newtonian fluids the peak in $\overline{u'^2}$ is always at $r>R_1$, but for the other two components of turbulence the peaks are at $r<R_1$ for *ER*=1.538 and at $r>R_1$ for *ER*=2. For the xanthan gum solutions this behaviour is confirmed with few modifications: the peaks in $\overline{u'^2}$ tend to occur closer to $r\approx R_1$ than with the Newtonian fluids, and for $\overline{w'^2}$ in the *ER*=1.538 expansion only for the profile at $x/h = 0.93$ the peak is at $r<R_1$.

Observation of Figs. 10–13 and comparison with the corresponding plots for the *ER*=1.538 expansion of Pereira and Pinho (2000) yields the following conclusions:

- The earlier development of $\overline{u'^2}$ for xanthan gum in comparison with the water flows (c.f. Fig. 10 where the data at $x/h = 0.93$ in Fig. 10b, c are slightly higher than in Fig. 10a in the region $-0.1<r'<0.4$) and the subsequent faster decay of this turbulent component relative to that of the Newtonian fluids is more pronounced in the larger than in the smaller expansion. In Fig. 11, at x= 0.3 m ($x/h\approx$23.1), $\left(\overline{u}'^2/U_1^2\right)$ has values around 0.005, whereas at the corresponding normalised location for *ER*=1.538 (x=0.16 m in Fig. 10 of Pereira and Pinho (2000)) maximum values of $\left(\overline{u}'^2/U_1^2\right)$ still exceed 0.02.
- As with the axial turbulence, for the radial normal Reynolds stress ($\overline{v'^2}$) the peak value occurs earlier in space with xanthan gum than with water (by about 20% in x/d, c.f. Fig. 13). This effect is again more pronounced in the *ER*=2 case since, in terms of step height, the peak $\overline{v}'^2$ in the small expansion occurs at x/h of 0.78 and 0.86 for the XG and water flows, respectively, whereas in the large expansion it occurs at 0.71 and 0.82, respectively. However, the maximum values of the stress for the two types of fluids do not differ significantly in contrast to the findings for the axial component of turbulence.
- For the tangential component of turbulence the effect of the expansion ratio is reversed: with the increase in the expansion ratio, the difference between the Newtonian and the non-Newtonian flow characteristics is reduced.
- Downstream of the region of peak turbulence the rate of dissipation of turbulent kinetic energy is faster with

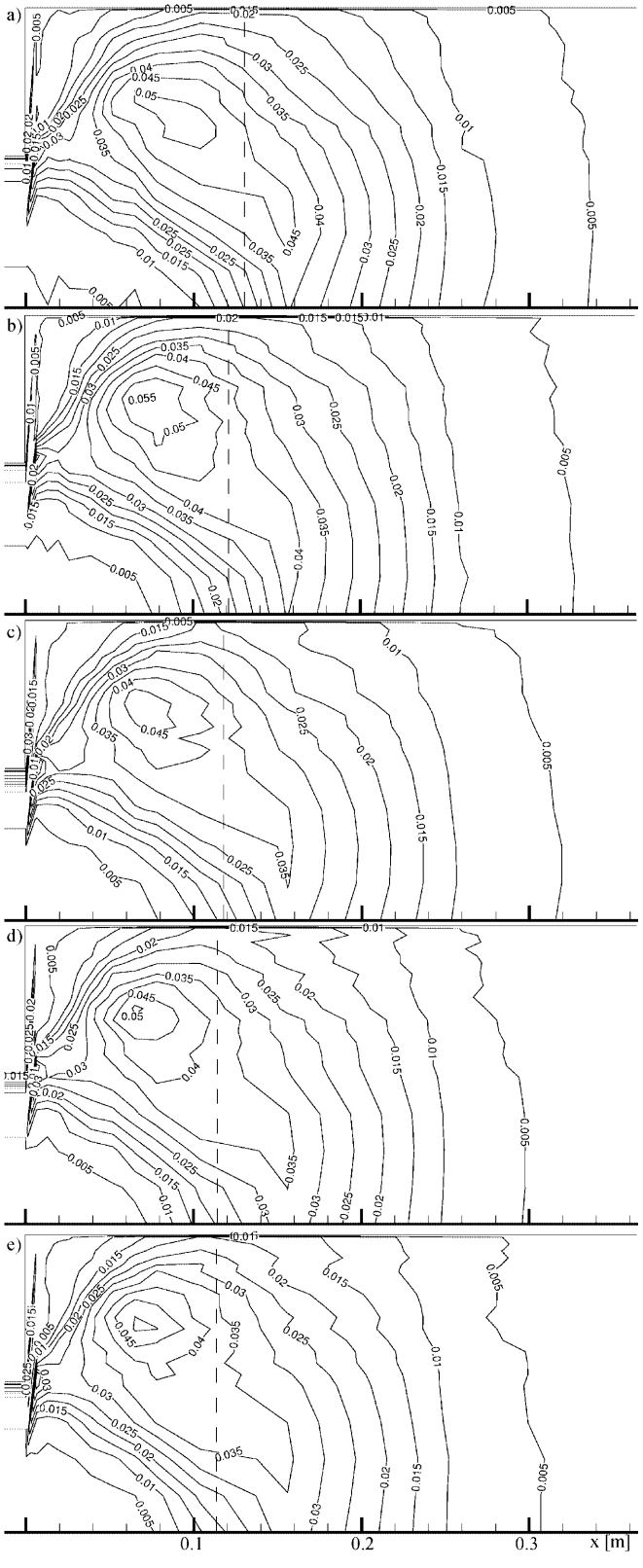

Fig. 11a–e. Contours of normalised $\overline{u'^2}$ for *ER*=2: **a** water, *Re*=50,400; **b** water, *Re*=134,000; **c** 0.1% XG, *Re*=19,600; **d** 0.2% XG, *Re*=19,400; **e** 0.2% XG, *Re*=27,100

the non-Newtonian fluids, and consequently their turbulence drops more than that of the Newtonian fluids. At x=0.2 m in Fig. 11 $\bar{u}'^2/U_1^2$ still exceeds 0.03 for the Newtonian fluids, but is always less than 0.025 for the xanthan gum solutions (a difference of 20%). For the $\bar{w}'^2$ and $\bar{v}'^2$ components the relative difference

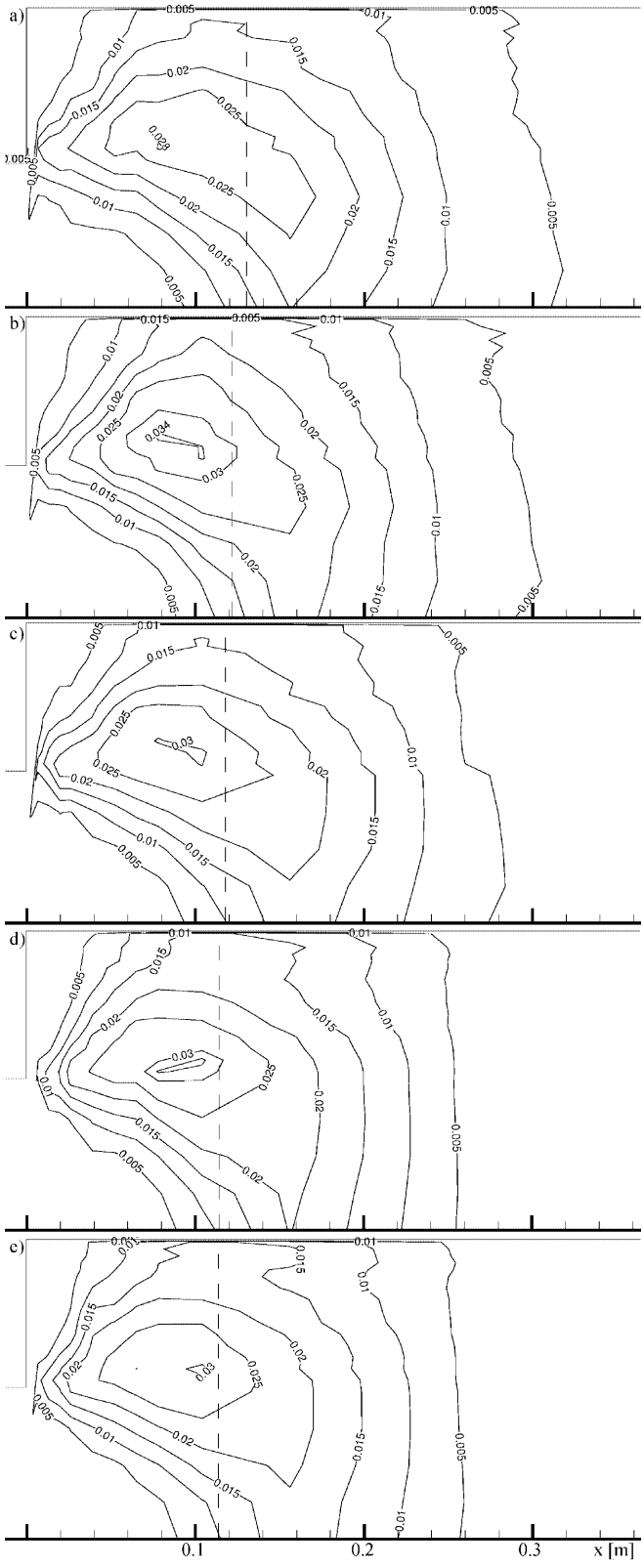

Fig. 12. Contours of normalised $\overline{w'^2}$ for ER=2: **a** water, *Re*=50,400; **b** water, *Re*=134,000; **c** 0.1% XG, *Re*= 19,600; **d** 0.2% XG, *Re*=19,400; **e** 0.2% XG, *Re*=27,100

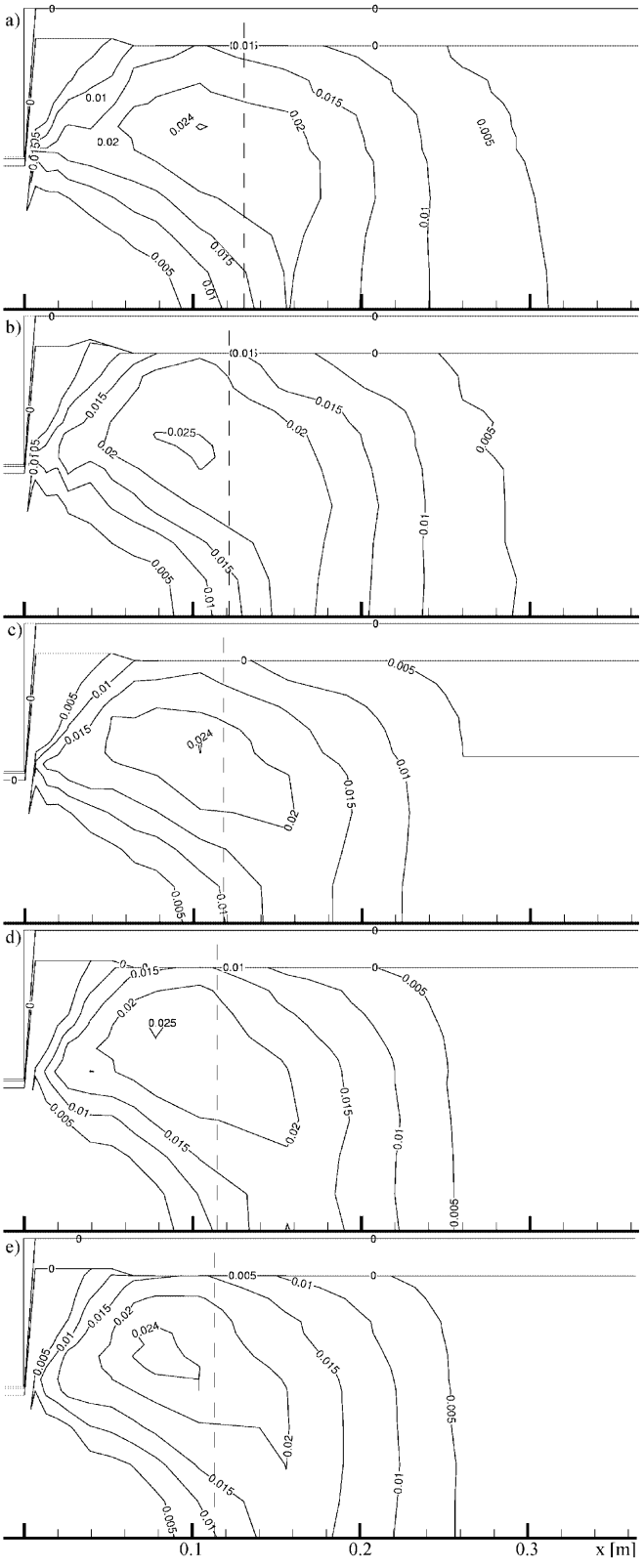

Fig. 13. Contours of normalised $\overline{v'^2}$ for ER=2: **a** water, *Re*=50,400; **b** water, *Re*=134,000; **c** 0.1% XG, *Re*=19,600; **d** 0.2% XG, *Re*=19,400; **e** 0.2% XG, *Re*=27,100

increases to about 25%. A comparison of the locations of the smallest contours of 0.005 in Figs. 11–13 also illustrates the point.

The differences between the Newtonian and non-Newtonian features of $\overline{u'^2}$ and $\overline{v'^2}$ both contribute to the decrease of the recirculation length of the xanthan gum solutions, but the relative behaviour of the tangential turbulence goes against this variation. Consequently, although the overall effect is still a reduction in recirculation length, the effect is less pronounced than in the smaller expansion.

The differences between ER=1.538 and ER=2 reported for $\overline{u'^2}$ result from the role that advection plays in this flow and the effect of confinement by the downstream wall. The advection of the higher axial turbulence from the upstream pipe wall region is responsible for the higher levels of axial turbulence immediately downstream of the expansion plane, and its peaks are closer to $r \approx R_1$ for the xanthan gum solutions than for Newtonian fluids. The increase in expansion ratio results in more physical space on the slow-moving side of the shear layer, and the free shear layer is seen to spread faster to the outside, thus raising the turbulence in the recirculation region.

The higher axial turbulence that develops with the increase in the expansion ratio from 1.538 to 2 is not mirrored in increases of the other normal Reynolds stresses and especially of the radial turbulence which, together with $\overline{uv}$ are the two most important components of Reynolds stress tensor that transfer momentum radially. Unfortunately, it is not possible to measure $\overline{uv}$ in this geometry using a single component LDV, and the variation of $\overline{uv}$ downstream of the expansion plane for the xanthan gum solutions is unclear. However, as with the other components of the Reynolds stress tensor, a significant part of $\overline{uv}$ in the near shear layer must be advected from the upstream pipe wall region. Now, it is known from the literature on pipe drag reduction with viscoelastic fluids that $\overline{uv}$ is significantly reduced in comparison with that for the pure Newtonian solvent at the same wall Reynolds number. Since our xanthan gum solutions are known to exhibit drag reduction, it is our belief that $\overline{uv}$ downstream of the expansion will be lower than for the corresponding water flows. Second, the decrease in the radial gradients of mean axial velocity that accompany the increase in expansion ratio will reduce production of $\overline{uv}$. This decoupling of $\overline{u'^2}$ and $\overline{v'^2}$ will be reflected in these quantities and so it is not surprising that, although $\overline{u'^2}$ increased with expansion ratio, $\overline{v'^2}$ did not. Similar behaviour has been observed by Berman and Tan (1985) and Luchik and Tiederman (1988) for channel and axisymmetric jet flows, respectively. Hence, the viscoelastic reduction in L/h relative to the Newtonian length becomes less pronounced with the larger expansion.

To a large extent, these features are due to the inlet condition of transverse turbulence coupled with the mechanisms of turbulence production in this axisymmetric flow. The transport equations of the Reynolds stress (Hinze 1975) in cylindrical coordinates show no direct production of $\overline{w'^2}$ and a production of $\overline{v'^2}$ that is smaller than the production of $\overline{u'^2}$ in the near shear layer (production of $\overline{v'^2}$ involves radial gradients of the radial mean velocity, whereas production of $\overline{u'^2}$ is proportional to the larger radial gradients of the axial mean velocity). However, the transverse normal stresses are not much smaller than $\overline{u'^2}$ because its production increases as the shear layer grows and because of the second mechanism contributing to $\overline{w'^2}$ and $\overline{v'^2}$, which is the redistributive role of pressure strain. This explains the latter peak values of these turbulence components relative to the location of the peak axial turbulence.

5 Conclusions

Measurements of the mean and turbulent flow characteristics of viscoelastic fluids in a sudden expansion with expansion ratio ER of 2.0 were carried out by means of laser-Doppler velocimetry and the results compared with those obtained by Pereira and Pinho (2000) in the ER=1.538 expansion, operating with the same fluids. In all cases the inlet condition was that of fully developed flow and the non-Newtonian fluids were aqueous solutions of xanthan gum at concentrations of 0.1 and 0.2 wt.%. These solutions were shear-thinning and exhibited elasticity in rheological flows (Coelho and Pinho 1998). Other evidence of elastic effects was reported by Pereira and Pinho (1999).

The main findings were:

- The higher levels of $\overline{u'^2}$ in the beginning of the shear layer were due to advection of higher upstream wall turbulence and higher $\overline{u'^2}$ production.
- The earlier development of $\overline{u'^2}$ and the subsequent faster decay of this turbulent component relative to that of the Newtonian fluids was more intense in the ER=2 expansion than in the smaller expansion. Similarly, for the radial normal Reynolds stress ($\overline{v'^2}$) the maximum turbulence occurred earlier with xanthan gum than with water. This effect was more pronounced in the ER=2 case, but the maximum values of this stress for the two types of fluids did not differ significantly in contrast to what happened in the ER=1.538 expansion.
- For the tangential component of turbulence the effect of the expansion ratio was reversed: with the increase in the expansion ratio the difference between the Newtonian and non-Newtonian characteristics was reduced. Thus, the differences between the Newtonian and non-Newtonian behaviour of $\overline{u'^2}$ and $\overline{v'^2}$ contributed to the decrease in the recirculation length of the xanthan gum solutions, but the relative behaviour of the tangential turbulence went against this variation. Consequently, although the overall effect was still a reduction in recirculation length, the effect was less pronounced in the ER=2 geometry than in the smaller expansion.

References

Berman NS; Tan H (1985) Two-component laser-Doppler velocimeter studies of submerged jets of dilute polymer solutions. AIChE J 31: 208–215

Castro OS; Pinho FT (1995) Turbulent expansion flow of low molecular weight shear-thinning solutions. Exp Fluids 20: 42–55

Coelho PM; Pinho FT (1998) Rheological characteristics of some diluted aqueous polymer solutions (in Portuguese). Mecânica Exp 3: 51–60

Escudier MP; Smith S (1999) Turbulent flow of Newtonian and shear-thinning liquids through a sudden axisymmetric expansion. Exp Fluids 27: 427–434

Escudier MP; Gouldson IW; Pereira AS; Pinho FT (1998) On the consistency of the rheology of dilute shear-thinning elastic fluids. Internal report of the Departments of Mechanical Engineering of the University of Liverpool, UK and Department of Mechanical Engineering and Industrial Management of the Faculty of Engineering of the University of Porto, Portugal

Escudier MP; Gouldson I; Pereira AS; Pinho FT; Poole RJ (2001) On the reproducibility of the rheology of shear-thinning liquids. J Non-Newt Fluid Mech 97: 99–124

Hinze JO (1975) Turbulence. McGraw-Hill, New York

Khezzar L; Whitelaw JH; Yianneskis M (1985) An experimental study of round sudden expansion flows. In: Proc 5th Symp on Turbulent Shear Flows, Cornell University, Ithaca, USA, pp 5–25

Lawn CJ (1971) The determination of the rate of dissipation in turbulent pipe flow. J Fluid Mech 37: 477–505

Luchik TS; Tiederman WG (1988) Turbulent structure in low concentration drag-reducing channel flows. J Fluid Mech 190: 241–263

Pak B; Cho YI; Choi SU (1990) Separation and reattachment of non-Newtonian fluid flows in a sudden expansion pipe. J Non-Newt Fluid Mech 37: 175–199

Pak B; Cho YI; Choi SU (1991) Turbulent hydrodynamic behavior of a drag-reducing viscoelastic fluid in a sudden expansion pipe. J Non-Newt Fluid Mech 39: 353–373

Pereira AS; Pinho FT (1999) Bulk characteristics of some variable viscosity polymer solutions in turbulent pipe flow. In: Technical Sessions on Rheology (SR26), COBEM99, XV Brasilian Congress of Mechanical Engineering, Águas de Lindóia SP, Brasil, 22–26 November

Pereira AS; Pinho FT (2000) Turbulent characteristics of shear-thinning fluids in recirculating flows. Exp Fluids 28: 266–278

Pereira AS (2000) Flow of non-Newtonian fluids in axisymmetric sudden expansions. PhD Thesis, University of Porto, Portugal (in Portuguese)

Pinho FT; Whitelaw JH (1990) Flow of non-Newtonian fluids in a pipe. J Non-Newt Fluid Mech 34: 129–144

Pronchick SW; Kline SJ (1983) An experimental investigation of the structure of turbulent reattachment flow behind a backward-facing step. Report MD-42, Thermosciences Div, Mech. Eng. Dept., Stanford University, Stanford, USA

Stieglmeier M; Tropea C (1992) A miniaturized, mobile laser-doppler anemometer. Appl Opt 111: 4096–4099

Virk PS; Mickley HS; Smith KA (1967) The ultimate asymptote and mean flow structure in Toms phenomena. J Appl Mech 92: 488–493

Virk PS (1975) Drag reduction fundamentals. AIChE J 21: 625–656